Resistivity of REBCO tapes in overcritical current regime: impact on superconducting fault current limiter modeling

N. Riva[1], F. Sirois[3], C. Lacroix[3], W.T.B de Sousa [2], B. Dutoit[1],F. Grilli[2]

[1] Ecole Polytechnique Fédérale de Lausanne, Switzerland
[2] Karlsruhe Institute of Technology, Germany
[3] Polytechnique Montréal, Canada

E-mail: nicolo.riva@epfl.ch

Abstract. A detailed knowledge of the resistivity of high-temperature superconductors in the overcritical current regime is important to achieve reliable numerical simulations of applications such as superconducting fault current limiters. We have previously shown that the combination of fast pulsed current measurements and finite element analysis allows accounting for heating effects occurring during the current pulses. We demonstrated that it is possible to retrieve the correct current and temperature dependence of the resistivity data points of the superconductor material. In this contribution, we apply this method to characterize the resistivity vs. current and temperature of commercial REBCO tapes in the overcritical current regime, between 77 K and 90 K and in self-field conditions. The self-consistency of the overcritical resistivity model $\rho_{\mathrm{OC}}(I,T)$ is verified by comparing DC fault measurements with the results of numerical simulations using this model as input. We then analyze by numerical simulation to what extent using the $\rho_{\mathrm{OC}}(I,T)$ model instead of the widely used power-law model $\rho_{\mathrm{PWL}}(I,T)$ affects the thermal and electrical performance of the tapes in the practical case of a superconducting fault current limiter. A remarkable difference is observed between the measured overcritical current resistivity model $\rho_{\mathrm{OC}}(I,T)$ and the power-law resistivity model $\rho_{\mathrm{PWL}}(I,T)$. In particular, the simulations using the power-law model show that the device quenches faster than with the overcritical resistivity model. This information can be used to optimize the architecture of the stabilizer in superconducting fault current limiters.

1. Introduction

Short-circuit currents can exceed the nominal current of a power system by more than ten times [1], and they are steadily increasing as new power generation is added in the networks. High fault currents put existing equipment at risk, so the use of superconducting fault current limiters (SFCL) becomes more and more important in future grids to protect them from these high energy faults. In this paper, we consider resistive SFCLs based on HTS REBCO tapes (RSFCL). In normal conditions, the

current in the power system stays below the critical current I_c of the SFCL, which then operates in the superconducting state with negligible electrical resistance. During a fault, if the short-circuit current exceeds I_c, the resistance rapidly increases and drives the SFCL into the normal state, where the overall resistance of the device limits the short-circuit current. The materials of the device must be designed to withstand the high increase of temperature for the time required by the circuit breaker to clear the fault [1]. Through finite element analysis (FEA), it is possible to study the electro-thermal behavior of the SFCL during the fault and estimate the maximum temperature in the device, as well as the current sharing between the various layers of the superconducting tape. Those quantities can be reliably estimated by simulation only with a good knowledge of all the material properties, in particular those of the superconductor, including their temperature dependence. Even though the electrical and thermal properties of materials such as silver, copper and Hastelloy are well documented in the literature [2], it is difficult to have an accurate knowledge of the overcritical current resistivity ($I > I_c$) of the superconducting material. Some authors have studied the electro-thermal behavior of SFCL during a fault using a power-law resistivity model [3,4], and others use a piecewise power-law in which the flux-flow is treated similarly to a flux creep region, but with a lower n-value [5]. These descriptions of the superconductor at high electric field remains very empirical. In previous works of ours, we showed that the combination of fast-pulsed current measurements (PCM) and FEA allows accurately extracting the overcritical current resistivity curve [6,7]. In this contribution, we analyze by means of simulation to what extent using the overcritical current model instead of the power-law model impacts the quench dynamics of an HTS tape used in a SFCL application. In the first part of the paper, we present the overcritical current resistivity model $\rho_{\mathrm{OC}}(J,T)$ of two SuperPower samples, determined experimentally. The PCM were carried out in liquid nitrogen at 77 K and in self-field conditions on the two samples, which are referred to as SP01 and SP02a in this paper. In the second part of the paper, we describe a model implemented in COMSOL Multiphysics, which was used to verify the consistency of the overcritical resistivity model with DC fault measurements, performed on a third sample named SP02b. The same model is used to evaluate the SFCL behavior in typical DC and AC fault current limitation scenarios, and the impact of using the overcritical current resistivity $\rho_{\mathrm{OC}}(J,T)$ instead of the commonly used power-law $\rho_{\mathrm{PWL}}(J,T)$ impacts the simulation results.

2. Resistivity curves in the overcritical current regime

In this section, we present the experimental setup used to characterize the REBCO tapes and the experimental curves post-processed with FEA. More specifically, after having characterized the REBCO tapes using PCM, we used the so-called Uniform Current (UC) model [6, 7] to process the experimental data and estimate the temporal evolution of the temperature profile across the thickness of a tape, as well as the amount of current flowing in each layer. This allows us to obtain an accurate value of the REBCO

resistivity as a function of current and temperature, noted $\rho_{\mathrm{OC}}(I_{\mathrm{REBCO}}, T)$. In this work, we determine $\rho_{\mathrm{OC}}(I_{\mathrm{REBCO}}, T)$ rather than $\rho_{\mathrm{OC}}(J_{\mathrm{REBCO}}, T)$. In the rest of this paper, we indicate $\rho_{\mathrm{OC}}(I_{\mathrm{REBCO}}, T)$ simply as $\rho_{\mathrm{OC}}(I, T)$.

2.1. Critical temperature, critical current and pulsed current measurements setup

In the critical temperature setup, the tapes were clamped between two copper blocks immersed in liquid nitrogen. A calibrated heating system allowed changing the temperature of the copper block while injecting 100 mA in the HTS tape. The resistance and temperature were recorded to determine $R_{\mathrm{Tape}}(T)$ [8].
The critical current I_{c} was measured by means of electrical transport measurements, with the experimental setup described in [9]. The sample holder was placed in a helium-gas flow cryostat that provided stable temperatures between 1.8 K and 200 K. The temperature was monitored with a Cernox sensor placed on the sample holder, while the current was injected in the sample up to the value at which the voltage corresponding to a critical electric field $E_{\mathrm{c}} = 10\,\mu\mathrm{V\,cm^{-1}}$ was reached on the length of the measured sample, namely 10 cm. PCM were performed in liquid nitrogen bath (77 K) on the samples utilizing the system reported in [10, 11], without damaging the tapes. Current pulses as short as 75 µs were injected in both samples, with current magnitude up to $I = 4.4\,I_{\mathrm{c}}$ and $200\,\mathrm{V\,m^{-1}}$ for SP01, and up to $I = 3.7\,I_{\mathrm{c}}$ and $140\,\mathrm{V\,m^{-1}}$ for SP02a. The characteristics of the silver-stabilized samples are given in Table 1.

Samples characteristics from SuperPower datasheet				
Sample	width w_{tape}	Thickness Silver h_{Ag}	Thickness REBCO h_{REBCO}	Thickness Hastelloy h_{Hast}
SP01/SP02a	4 mm	2 µm/2.2 µm	1 µm	50 µm
Samples characteristics from measurements				
Sample	Length l_{tape}	Critical current I_{c}	Critical temperature T_{c}	n-value
SP01	10 cm	57 A	88 K	25
SP02a	10 cm	110 A	90 K	30

Table 1: Characteristics of the two SuperPower samples. The critical current, critical temperature and n-value were measured in self field condition at 77 K.

2.2. Regularized overcritical current data

The raw overcritical data are shown in Figure 1. The scattered red-dots correspond to experimental points obtained with the PCM and post-processed with the UC model (see [6, 7]), while the blue points correspond to critical current measurements. In [6], we reported a $\rho_{\mathrm{OC}}(I, T)$ data set whose validity was restricted to a limited range of currents and temperatures. This was because data interpolation had its limitations

for reconstructing surfaces suitable for FEA from experimental measurements. Due to the limited range of experimental data and the need to prevent ill-posed problem or overfitting, a regularization [12] of the raw data is required. The detailed procedure to regularize the data goes beyond the scope of the paper and will be published on its own elsewhere. Figure 1 presents the $\rho_{\mathrm{OC}}(I,T)$ surfaces obtained from two experimental data sets.

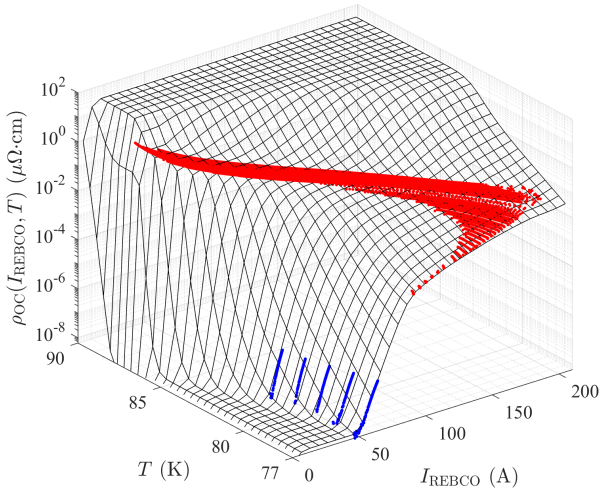

(a) Regularized resistivity surface for sample SP01.

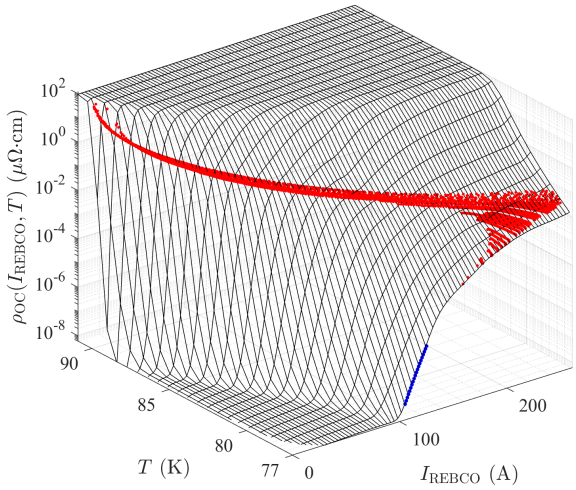

(b) Regularized resistivity surface for sample SP02a.

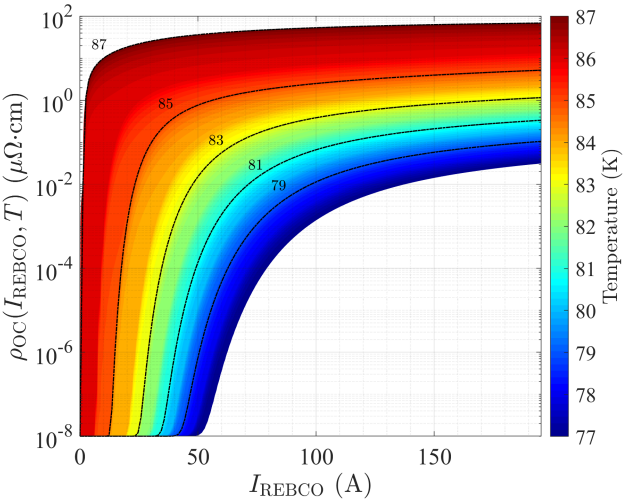

(c) Regularized isothermal resistivity curves for sample SP01.

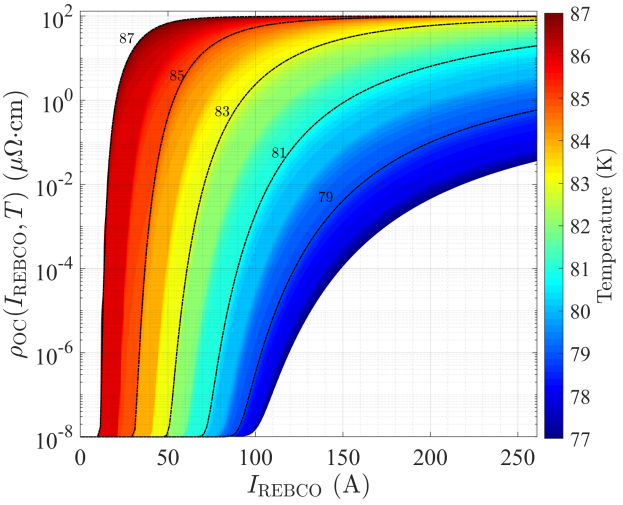

(d) Regularized isothermal resistivity curves for sample SP02a.

Figure 1: Resistivity surfaces (a)-(b) and isothermal curves (c)-(d) reconstructed through data regularization of the measurements for samples SP01 and SP02a. The scattered red dots (a)-(b) correspond to experimental points obtained using PCM and post-treated using the UC model (see [6,13] for detailed procedure), while the blue points are from the critical current measurements. The curves in (c)-(d) show the $\rho_{\mathrm{OC}}(I)$ resistivity curves for different temperatures.

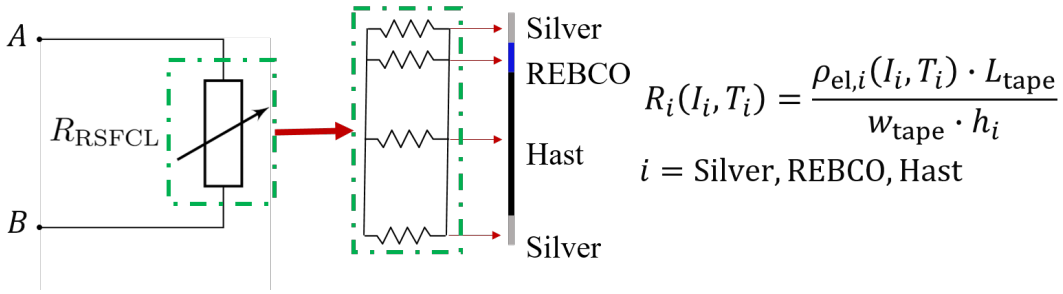

Figure 2: Schematic representation of the HTS tape model implemented in COMSOL Multiphysics.

3. Self-consistency check of the overcritical resistivity model

3.1. Numerical models

In order to verify the correctness of the overcritical resistivity model obtained above, and also to study the behavior of REBCO tapes in various quench scenarios, we use a 1-D thermal finite element model (temperature variation across the thickness of the tape) coupled with an electric circuit model (current sharing between the various layers of the tape). We assume that the simulated tapes and thermal properties of the conductor do not vary significantly along their width and length. This means that the simulated tapes have uniform properties and that with this simple model one cannot investigate the impact of defects and hot-spots on the RSFCL behavior. The model is nevertheless sufficiently accurate to study short samples. The equivalent 1-D electrical model of the RSFCL is represented in Figure 2. The RSFCL is modeled as a set of resistors in parallel, representing the stabilizer (in this case silver), the Hastelloy and the REBCO layers, respectively. Each resistor $R_i(I_i, T_i)$ is defined by the electrical resistivity $\rho_{\mathrm{el,i}}(I_i, T_i)$, the length of the the tape L_{tape}, its width w_{tape} and the thickness of the single layer h_i, where the subscript i stands for the layer of the tape (i.e. silver, REBCO, etc.). A voltage V_{app} or a current I_{app} can be applied across the tape terminals A and B.

The model is implemented in COMSOL Multiphysics. The heat equation, modeled in the Heat Transfer Module (ht), is coupled with the equivalent circuit model of the RSFCL, modeled in the Electric Circuit Module (cir) [14]. The heat equation is solved on each 1-D domain, schematically represented in Figure 2, and reads as follows:

$$\rho_{\mathrm{mass},i}(T_i) C_{\mathrm{p},i}(T_i) \frac{\partial T_i}{\partial t} + \frac{\partial}{\partial x}\left(- k_i(T_i) \frac{\partial T_i}{\partial x} \right) = \frac{R_i(I_i, T_i) \cdot I_i^2}{\Omega_i} - h_{\mathrm{LN_2}} \cdot (T_i - T_0) \Big|_{\partial\Omega}, \qquad (1)$$

where on the left side we have the mass density $\rho_{\mathrm{mass},i}(T_i)$, the specific heat capacity $C_{\mathrm{p},i}(T_i)$ and the thermal conductivity $k_i(T_i)$. On the right side of equation, there is the heat source term and a cooling term. The heat source comes from Joule's first law, i.e. $P = R_i \cdot I_i^2 / \Omega_i$, and the volume of the conductor is noted as $\Omega_i = w_{\mathrm{tape}} \cdot L_{\mathrm{tape}} \cdot h_i$. The heat exchange with the liquid nitrogen is taken into account applying a boundary condition applied only on the top and the bottom layers of the tape (silver surfaces), indicated

by $\partial\Omega$. In Equation (1), the heat transfer coefficient $h_{\mathrm{LN_2}}(T_i - T_0)$ is a function of the temperature [15]. For better readability, the temperature dependence of $h_{\mathrm{LN_2}}(T_i - T_0)$ is omitted and the transfer coefficient is simply written as $h_{\mathrm{LN_2}}$. The temperature dependence of all the thermal and electrical material properties are taken into account. For R_{REBCO}, we consider the dependence of its resistivity with temperature and current using the overcritical resistivity models introduced above. The overcritical current curves $\rho_{\mathrm{OC}}(I, T)$ are implemented with a look-up table. For purpose of comparison, we also use a power-law model with a temperature dependent critical current $I_{\mathrm{c}}(T)$. We write the power-law as follows:

$$\rho^{\mathrm{SC}}_{\mathrm{PLW}}(I, T) = \frac{E_{\mathrm{c}}}{I_{\mathrm{c}}(T)} \left(\frac{|I|}{I_{\mathrm{c}}(T)} \right)^{n-1},$$

where $E_{\mathrm{c}} = 1\,\mu\mathrm{V\,cm^{-1}}$ is the electric field criterion, n is the power-law exponent and $I_{\mathrm{c}}(T)$ is given by a relationship of the form:

$$I_{\mathrm{c}}(T) = I_{\mathrm{c,77\,K}} \cdot \frac{T_{\mathrm{c}} - T}{T_{\mathrm{c}} - 77\,\mathrm{K}}. \tag{2}$$

The normal state resistivity $\rho_{\mathrm{NS}}(T)$ of REBCO is added in parallel to the power-law, in order to obtain a total resistivity that better reproduces the electrical behavior of REBCO [16] over a wide temperature range, i.e.

$$\rho_{\mathrm{PLW}} = \frac{\rho_{\mathrm{PLW}}(I, T) \cdot \rho_{\mathrm{NS}}(T)}{\rho_{\mathrm{PLW}}(I, T) + \rho_{\mathrm{NS}}(T)}. \tag{3}$$

The temperature dependence of the normal-state resistivity of REBCO is modeled with a simple linear relationship [17], i.e.:

$$\rho_{\mathrm{NS}}(T) = \rho_{T_{\mathrm{c}}} + \alpha \cdot (T - T_{\mathrm{c}}),$$

where $\rho_{T_{\mathrm{c}}} = 100\,\mu\Omega\,\mathrm{cm}$ and $\alpha = 0.47\,\mu\Omega\,\mathrm{cm\,K^{-1}}$ [18].

3.2. DC fault current measurements

DC fault current measurements in a liquid nitrogen bath (77 K) were performed on a tape called SP02b. The SP02b sample was 13.5 cm long, obtained from the same spool as the SP02a sample (1.1 µm of surrounding silver stabilizer, $I_{\mathrm{c}} = 110\,\mathrm{A}$ at 77 K in self-field conditions). The experimental setup used is schematically represented in Figure 3. The voltage was applied on the sample with a capacitor previously charged with a current source. A transistor was used as a switch to trigger the discharge. The capacitor could generate currents as high as 1600 A in the circuit. We measured the voltage drop V_{shunt} across a calibrated resistor R_{shunt} in order to determine the current in the circuit as $I_{\mathrm{app}} = V_{\mathrm{shunt}}/R_{\mathrm{shunt}}$. Finally, we measured the voltage V_{HTS} with the help of voltage taps installed on the sample, separated by a distance of 9.5 cm. Each voltage tap was located 1 cm away from the copper terminals, which was sufficient to allow the current

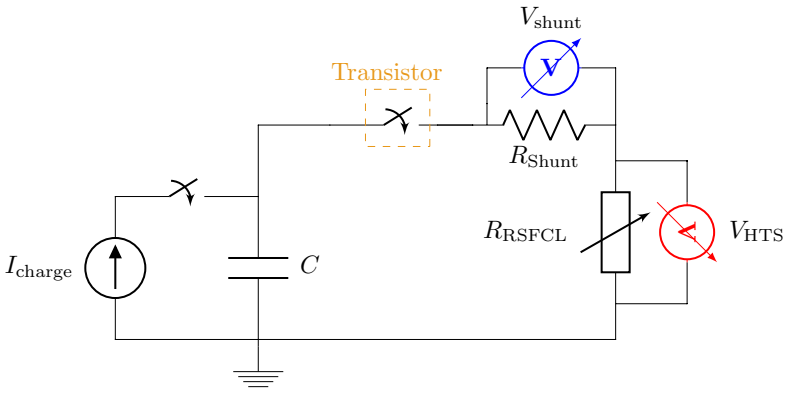

Figure 3: Schematic representation of the experimental setup.

transfer into the superconducting layer. The electric field and current for two limitations tests are presented in Figure 4. In Figure 4(left), the voltage applied on the sample was 3.02 V, which generated a peak current of $I_{\text{peak}} = 184.5$ A. In Figure 4(right) the voltage applied on the sample was 3.23 V, which generated a peak current of $I_{\text{peak}} = 189$ A. In this figure $E_{\text{app}} = V_{\text{app}}(t)/L$, where L is the spacing between voltage taps (9.5 cm), is represented in green on the right axis of the figure. We observe that the behavior can not be explained by spurious inductive signals and heating only. One hypothesis is that, since the current regime explored in these measurements is near or above the critical current of the tape (110 A), the inhomogeneous critical current distribution leads to the onset of localized normal resistive zones, hence to the abrupt change of slope in the observed voltage.

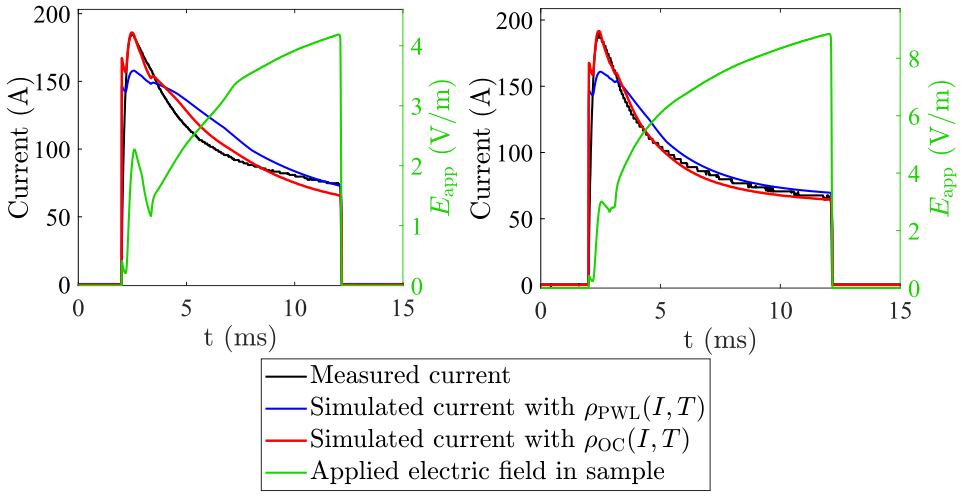

Figure 4: Measurements and simulations of an HTS tape undergoing fault current limitation under an increasing applied electric field. The current peak at the beginning which is very similar for the two electric fields level considered, $I_{\text{peak}} = 184.5$ A (left) and $I_{\text{peak}} = 189$ A (right) respectively. The measurements were performed on one sample (SP02b) coming from the same batch as SP02a.

3.3. Simulations vs. measurements

In Figure 4, the results of the experimental measurements and the COMSOL simulations are compared. The overcritical resistivity model ρ_{OC} was implemented in the numerical model described in Section 3.1 in order to assess its validity by comparing simulation results with the DC fault measurements. The measured voltage V_{HTS} was used as the voltage excitation $V_{\mathrm{app}}(t)$, across the terminals A and B in Figure 2. The electric-circuit used for self-consistency check is illustrated in Figure 5a. Overall, the model based on ρ_{OC} reproduces accurately the temporal profile of the measured current for the two electric fields level considered, especially the current peak at the beginning. For comparison, we also calculated the current with the power-law model. Unlike the ρ_{OC} model, the ρ_{PWL} model does not reproduce adequately the experimental curves.

4. Impact of resistivity model on SFCL behavior

In this section, we analyze the impact of using the overcritical current model instead of the power-law model. In particular, we calculate by simulation the temporal evolution of current and temperature in the tape for different homogeneous DC and AC fault current limitation conditions.

4.1. Impact on DC fault current limitation

Various fault conditions were generated by applying different values of DC voltage pulses, noted $V_{\mathrm{app}}(t)$ (Figure 5a). Two representative cases are plotted in Figure 6. We deliberately chosen two electric field values ($28.21\,\mathrm{V\,m^{-1}}$ and $28.26\,\mathrm{V\,m^{-1}}$), where the recovery of the tape was significantly different, to verify if using $\rho_{\mathrm{OC}}(I,T)$ instead of $\rho_{\mathrm{PWL}}(I,T)$ would have a significant impact. From Figure 6 we can conclude that for

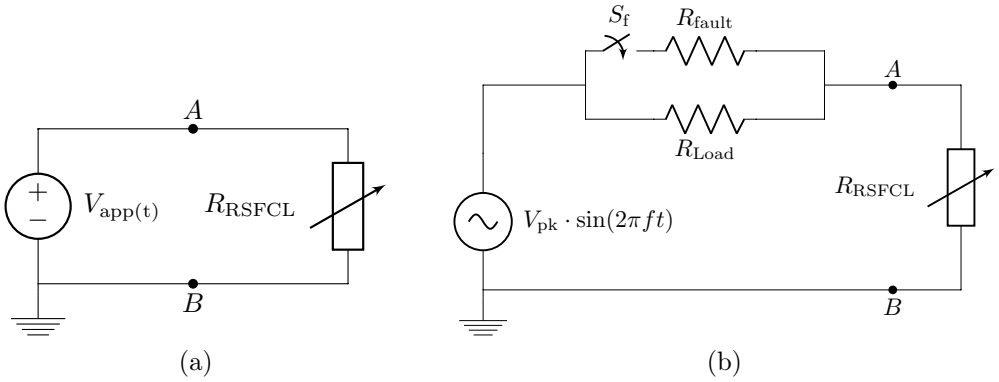

Figure 5: Signal excitations used in the model of Figure 2 to check (a) the self-consistency of the overcritical resistivity model, and (b) its impact on SFCL behavior.

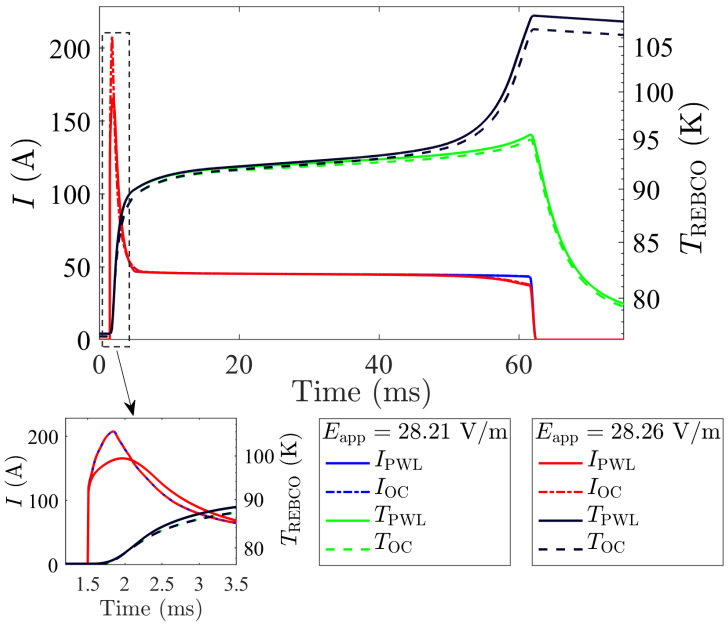

Figure 6: Simulated DC faults on SP02a with the overcritical resistivity model and the power-law model, for $E_{\mathrm{app}} = 28.21\,\mathrm{V\,m^{-1}}$ and $E_{\mathrm{app}} = 28.26\,\mathrm{V\,m^{-1}}$. The small difference between the two values of E_{app} leads to a drastic change in the recovery of the tape.

homogeneous DC fault conditions, there is not much difference. Since the heating occurs quickly at the beginning of the fault, the tape is no longer superconducting within a few ms, hence the stabilizer dominates the resistive behavior. However, similarly to what reported in Figure 4, a remarkable difference is present at the beginning of the pulse, where the peak of the limited current I_{OC} is larger than that of I_{PWL} (inset in Figure 6).

4.2. Impact on AC fault current limitation

The model used to simulate AC fault current limitation is presented in Figure 5b. A sinusoidal voltage signal is imposed on the circuit, while a load resistor R_{Load} draws the nominal current from the source. A switch in parallel to the load resistor, when closed, simulates the fault occurring at a given time and draws the fault current through a resistor R_{fault}. In the simulations, $V_{\mathrm{peak}} = 12\,\mathrm{V}$ and $f = 50\,\mathrm{Hz}$. The switch operates at $t = 20\,\mathrm{ms}$ and the short-circuit is cleared after two periods of the sinusoidal voltage source, i.e. $t = 60\,\mathrm{ms}$. Finally, the prospective current is calculated as $I_{\mathrm{fault}} = V_{\mathrm{peak}}/R_{\mathrm{fault}}$. In Figure 7, we present the evolution of the total current in the circuit and the current in the REBCO layer (top), the temperature (middle) and the REBCO layer resistivity (bottom). The difference in the simulations of the fault current when using $\rho_{\mathrm{OC}}(I,T)$ instead of $\rho_{\mathrm{PWL}}(I,T)$ is very small, except during the first peak, when $I_{\mathrm{fault}} = 1.63\,I_{\mathrm{c}}$, as shown in Figure 7a. As in the case of DC faults, the heating occurs rapidly at the beginning of the fault, and the device is no longer superconducting after a few ms, hence the stabilizer dominates the resistive behavior.

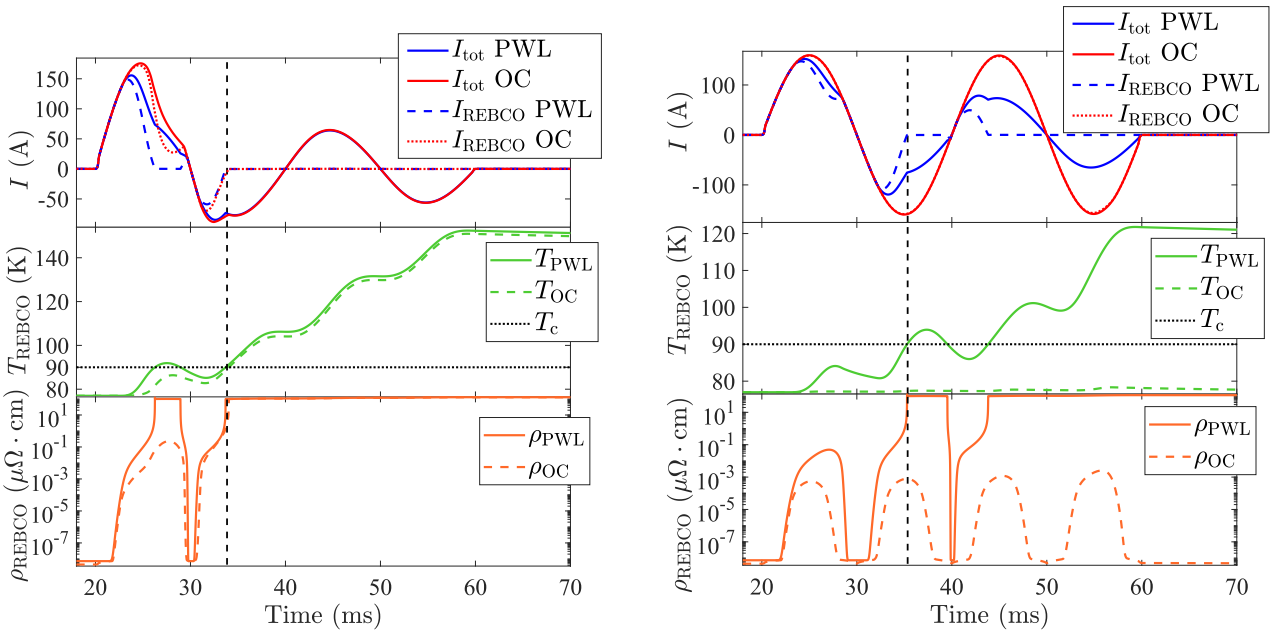

(a) $I_{\text{fault}} = 1.63\, I_c$ (b) $I_{\text{fault}} = 1.45\, I_c$

Figure 7: Simulated AC faults on SP02a with the overcritical resistivity model ρ_{OC} and the power-law model ρ_{PWL}, for (a) $I_{\text{fault}} = 1.63\, I_c$ and (b) $I_{\text{fault}} = 1.45\, I_c$. The black dashed lines indicate the moment where the quench occurs (a) for both models and (b) for ρ_{PWL}.

Figure 7b shows the results for $I_{\text{fault}} = 1.45\, I_c$. In this case, the difference in simulation results is remarkable. Even if the first current peak does not change considerably using $\rho_{OC}(I, T)$ instead of $\rho_{PWL}(I, T)$, the temperature rise is significantly different. With the power-law model, the tape quenches more rapidly, i.e. its temperature reaches $T_c = 90\,\text{K}$ in less than one cycle (see Figure 7b).

5. Discussion

The difference in the temperature rise obtained when using the overcritical current model instead of the power-law model can be understood by comparing the electrical resistance per unit of length of the of REBCO layer ($R_{\text{REBCO}}(I, T)/L_{\text{tape}}$), the total resistance per unit of length of the tape ($R_{\text{tape}}(I, T)/L_{\text{tape}}$) and the total Joule losses ($\sim R \cdot I^2$).

In Figure 8a, we plot $R_{\text{REBCO,PWL}}/L_{\text{tape}}$ described by the power-law model (full lines), compared with $R_{\text{REBCO,OC}}/L_{\text{tape}}$ described by the overcritical resistivity model (dashed lines). The constant line at $2.5\,\Omega\,\text{cm}^{-1}$ is the normal state resistance per unit length of REBCO at 90 K, while the black scattered points correspond to the experimental measurements. The difference between $R_{\text{REBCO,PWL}}(I, T)/L_{\text{tape}}$ and $R_{\text{REBCO,OC}}(I, T)/L_{\text{tape}}$ for the same current is striking. If we consider $I_{\text{REBCO}} = 200\,\text{A}$

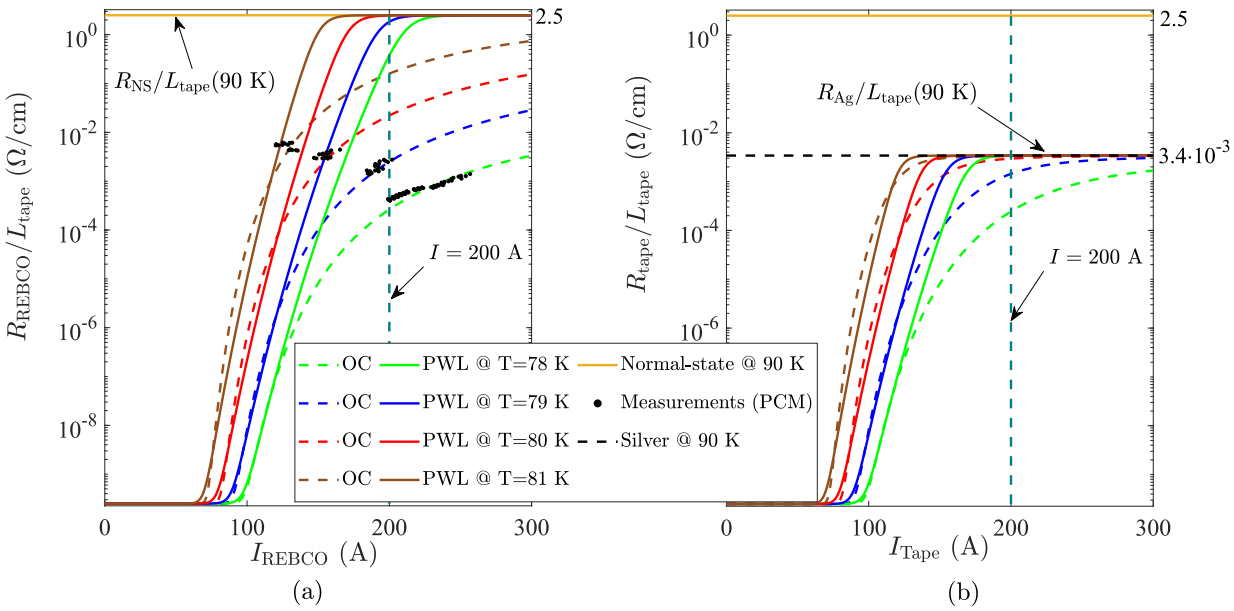

Figure 8: (a) Comparison between the power-law and the overcritical resistivity models in term of resistance per unit length. The normal state resistance of REBCO is considered in the model. (b) Comparison between the global resistance per unit length of the tape, using the power-law and the overcritical current model, in parallel with the resistance of silver at 90 K.

and $T = 78\,\mathrm{K}$, the ratio between the two resistances is:

$$\frac{R_{\mathrm{REBCO,PWL}}(200\,\mathrm{A}, 78\,\mathrm{K})/L_{\mathrm{tape}}}{R_{\mathrm{REBCO,OC}}(200\,\mathrm{A}, 78\,\mathrm{K})/L_{\mathrm{tape}}} = \frac{0.32\,\Omega\,\mathrm{cm}^{-1}}{2\cdot 10^{-4}\,\Omega\,\mathrm{cm}^{-1}} \simeq 1600.$$

When looking at the tape as a whole, this difference is mitigated by the presence of a stabilizer such as silver. In Figure 8b, the resistance per unit length of silver is represented as a constant line at $3.4\cdot 10^{-3}\,\Omega\,\mathrm{cm}^{-1}$. The silver acts as a parallel resistor and the effective resistance per unit length of the tape is lower than that of a single REBCO layer. In this case, the ratio between the two resistances is:

$$\frac{R_{\mathrm{tape,PWL}}(200\,\mathrm{A}, 78\,\mathrm{K})/L_{\mathrm{tape}}}{R_{\mathrm{tape,OC}}(200\,\mathrm{A}, 78\,\mathrm{K})/L_{\mathrm{tape}}} = \frac{3.4\cdot 10^{-3}\,\Omega\,\mathrm{cm}^{-1}}{2\cdot 10^{-4}\,\Omega\,\mathrm{cm}^{-1}} \simeq 17.$$

Therefore, when the prospective current is $I_{\mathrm{fault}} = 1.63\,I_{\mathrm{c}}$ (Figure 7a), the high current pushes the device in the normal state, far from the regime where the differences between the resistances is important. Since the temperature reaches the critical temperature $T_{\mathrm{c}} = 90\,\mathrm{K}$ at the beginning of the fault, what we are simulating is the current flowing in the silver stabilizer and the Hastelloy, which have the same properties in the two simulations. The situation for $I_{\mathrm{fault}} = 1.45\,I_{\mathrm{c}}$ is different. A better insight of the role played by the different resistivity models is given by the total Joule losses in the tape. The total losses can be written as $P_i = R_{\mathrm{tape}}\cdot J_i^2$. In Figure 9 we compare the total current, the resistance per unit length of the tape and the total Joule losses obtained

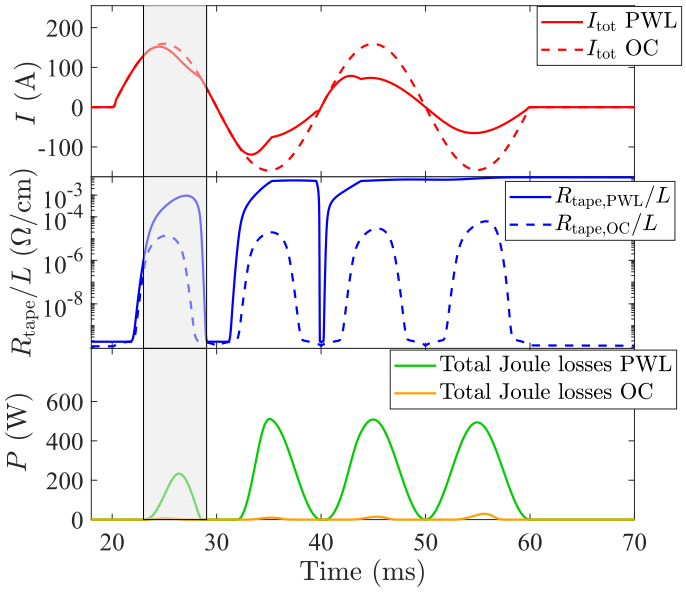

Figure 9: Comparison between the total current (top), resistance per unit length (middle) and Joule losses (bottom) in the RSFCL model using the power-law and overcritical current resistivity models in the AC current limitation case with $I_{\text{fault}} = 1.45\, I_{\text{c}}$. The gray-shaded area shows the remarkable difference in term of Joule losses.

with the power-law and overcritical current resistivity models. In the gray-shaded area between 23 ms and 29 ms, when the tape is still superconducting, we see that the total current $I_{\text{tot,PWL}}$ is not too different from $I_{\text{tot,OC}}$. However, we see that $R_{\text{tape,PWL}}$ is considerably larger than $R_{\text{tape,OC}}$ ($R_{\text{tape,PWL}} \simeq 100 \cdot R_{\text{tape,OC}}$). As a consequence, we have $P_{\text{PWL}} > P_{\text{OC}}$ and the temporal evolution of the temperature in the SFCL in the two case is very different. For $t > 45\,\text{ms}$, $R_{\text{tape,PWL}} \simeq R_{\text{Ag}} = 3.4 \cdot 10^{-3}\,\Omega\,\text{cm}^{-1}$ and the stabilizer dominates the resistive behavior. However, $R_{\text{tape,OC}}$ remains low, the device is still in the superconducting state. This situation clearly shows that scenarios where low overcurrent transients are involved are highly impacted by the correct choice of resistivity model. In this case, using the $\rho_{\text{PWL}}(I,T)$ model leads to a wrong estimation of the temporal evolution of the temperature.

6. Conclusions

In this paper, we demonstrated how an accurate knowledge of the overcritical current resistivity $\rho_{\text{OC}}(I,T)$ as a function of current and temperature is important when studying the electro-thermal behavior of RSFCL. Through numerical simulations, we evaluated the impact of using the overcritical current model (validated with DC fault current measurements) instead of the power-law model in the simple case of an RSFCL constituted of a silver-stabilized tape. We showed that, for low AC overcurrent faults the power-law model leads to a wrong estimation of the temporal evolution of the

temperature, largely overestimating the maximum temperature at the end of the AC fault. When using the overcritical current model, the temperature is much lower. This knowledge can be helpful in the design phase of a RSFCL, since the amount of stabilizer plays an important role on the total cost of the tape. Finally, since the model used in this paper assumes uniform material properties in the REBCO tape, it cannot be used to investigate the impact of defects and hot-spots. Therefore, further electro-thermal simulations capable of taking into account these aspects need to be carried out in order to refine this analysis.

Acknowledgments

This research was supported by Swiss Federal Office of Energy SFOE under grant agreement SI/500193-02. The authors want to thank Jason Nicholson from MathWorks for his expertise and advice that greatly facilitated this research.

References

[1] Tixador P 2018 *Superconducting Fault Current Limiter* (World Scientific) URL `https://www.worldscientific.com/doi/abs/10.1142/11062`
[2] Eichenauer W 1971 *Thermophysical Properties of Matter* (Wiley) URL `https://onlinelibrary.wiley.com/doi/abs/10.1002/bbpc.19710751034`
[3] Liang F, Yuan W, Baldan C A, Zhang M and Lamas J 2015 *Journal of Superconductivity and Novel Magnetism* **28** 2669–2681
[4] Czerwinski D, Jaroszynski L, Janowski T, Majka M and Kozak J 2014 *IEEE Transactions on Applied Superconductivity* **24** 5600104
[5] Paul W, Chen M, Lakner M, Rhyner J, Braun D and Lanz W 2001 *Physica C: Superconductivity* **354** 27–33
[6] Riva N, Richard S, Sirois F, Lacroix C, Dutoit B, Grilli F, Current A P and Pcm M 2019 *IEEE Transactions on Applied Superconductivity* **29** 6601705
[7] Richard S, Sirois F and Lacroix C 2019 *Journal of Applied Physics* **126** 023902
[8] Wu M K, Ashburn J R, Torng C J, Hor P H, Meng R L, Gao L, Huang Z J, Wang Y Q and Chu C W 1987 *Physical Review Letters* **58** 908–910
[9] Lao M, Hänisch J, Kauffmann-Weiss S, Gehring R, Fillinger H, Drechsler A and Holzapfel B 2019 *Review of Scientific Instruments* **90** ISSN 10897623
[10] Sirois F, Coulombe J, Roy F and Dutoit B 2010 *Superconductor Science and Technology* **23** 3–8 ISSN 09532048
[11] Sirois F, Coulombe J and Bernier A 2009 *IEEE Transactions on Applied Superconductivity* **19** 3585–3590 ISSN 10518223
[12] Nicholson J 2019 Introduction to Regularizing with 2D and 3D Data and Monotonic Constraints (Website) URL `https://mathformeremortals.wordpress.com`
[13] Richard S, Sirois F and Lacroix C *To be published*
[14] COMSOL Multiphysics® v. 5.4. (Website) URL `www.comsol.com`
[15] Roy F 2010 *Modeling and Characterization of Coated Conductors Applied to the Design of SFCL* Phd thesis
[16] Duron J, Grilli F, Dutoit B and Stavrev S 2004 *Physica C: Superconductivity* **401** 231–235
[17] Bonnard C h, Sirois F, Lacroix C and Didier G 2017 *Supercond. Sci. Technol.* **30** 014005
[18] Friedmann T A, Rabin M W, Giapintzakis J, Rice J P and Ginsberg D M 1990 *Physical Review B* **42** 6217–6221